Electrochemical Activation of Ni Catalysts with Potassium Ionic Conductors for CO_2 Hydrogenation

N. Gutierrez-Guerra[1] · J. Gonzalez-Cobos[1] · J. C. Serrano-Ruiz[2] · J. L. Valverde[1] · A. de Lucas-Consuegra[1]

Published online: 15 September 2015

Abstract Three different kind of Ni-based catalysts were prepared on a K-b$^{00}Al_2O_3$ solid electrolyte by combining the annealing of an organometallic paste and the addition of a catalyst powder. The different catalysts films were tested in the CO_2 hydrogenation reaction under electrochemical promotion by K? ions, and were characterized by XRD and SEM. The catalyst film derived from the addition of an a-Al_2O_3 powder to the Ni catalyst ink presented the highest catalytic activity as a result of the increase in Ni catalyst film porosity. The influence of the applied potential and other operation variables were evaluated on the Ni catalytic activity and selectivity. Hence, the CO production rate was enhanced either by decreasing the applied potential (with the consequent supply of K? ions to the catalyst surface) or by increasing the CO_2 (electron acceptor) feed concentration. On the other hand, CH_4 production rate was favoured at positive potentials (removing K? from the catalyst surface) or by increasing the H_2 (electron donor) feed concentration. The global CO_2 consumption rate increased upon negative polarization in all experiments and the electrochemical promotion of catalysis effect showed to be reversible and reproducible. Hence, the electrochemical promotion phenomena demonstrated to be a very useful technique to in situ modify and control the catalytic activity and selectivity of a non-noble metal such as Ni for the production of CH_4 or syngas via CO_2 valorization.

& A. de Lucas-Consuegra
antonio.lconsuegra@uclm.es

[1] Department of Chemical Engineering, School of Chemical Sciences and Technology, University of Castilla-La Mancha, Avda. Camilo Jose´ Cela 12, 13005 Ciudad Real, Spain

[2] Abengoa Research, Abengoa, C/Energ´ıa Solar no. 1, Palmas Altas, 41014 Sevilla, Spain

Keywords EPOC · CO_2 removal · Reverse water gas shift · Methanation · Ni catalyst · Syn-gas

1 Introduction

Different strategies are being developed to mitigate the global warming and climate change, some of them being focused on the separation, storage and utilization of the CO_2. In this sense, hydrogenation of CO_2 can be considered as one of the most important chemical conversion reactions, not only for the effective decrease of the overall CO_2 emissions but also for the production of many possible renewable fuels (hydrocarbons or alcohols) [1–3]. However, CO_2 is a thermodynamically stable compound and thus requires high activation energy for its transformation into other chemicals [4, 5]. Although numerous organic syntheses involve CO_2 as the feedstock, only a few have reached industrial commercialization, for instance, the production of urea and its derivatives, salicylic acid, and carbonates [1, 5]. Most studies on catalytic hydrogenation of CO_2 have been performed using metal catalysts (e.g. Pt, Rh, Pd, Ru, Cu, Fe, Co and Ni) supported on different oxides (e.g. Nb_2O_3, ZrO_2, Al_2O_3, SiO_2, and MgO) [6–10]. Depending on both the employed catalytic system (metal/support) and on the reaction conditions, different products can be obtained including CO, CH_4, formic acid, formaldehyde, dimethyl ether, methanol or higher alcohols [1, 4–6, 11, 12]. These catalytic reactions can be summarized according to the following scheme:

$$xCO_2 + (2x - z + y/2)H_2 \rightarrow C_xH_yO_z + (2x - z)H_2O \quad (1)$$

For instance, the reverse water gas shift (RWGS, Eq. 2) and CO_2 methanation (Eq. 3) reactions can be described as follows:

$CO_2 + H_2 \rightarrow CO + H_2O$ (2)

$CO_2 + 4H_2 \rightarrow CH_4 + 2H_2O$ (3)

Hence, the control of the catalyst selectivity toward the different hydrogenation products is highly required. In this sense, alkali promotion has been described to be an effective approach to improve the activity and/or selectivity of different metal catalysts [13]. For instance, the promoter effect of potassium in the CO_2 hydrogenation reaction has been previously studied over conventional heterogeneous catalysts [14, 15]. Both the activity and the selectivity of a metal or metal oxide catalyst film deposited on an ionic conductor can also be modified, in a significant, controlled and reversible manner, by electrically polarizing the catalyst-electrode via the effect of electrochemical promotion of catalysis (EPOC) also known as NEMCA effect (non-faradaic electrochemical modification of catalytic activity). This phenomenon was first observed by Stoukides and Vayenas [16] and is based on the controlled migration of promoting ions, e.g., O^{2-}, Na^{+}, K^{+} or H^{+} ions, from an electroactive support, such as b''-Al_2O_3 (a Na^{+} or K^{+} conductor), YSZ (yttrium-stabilized-zirconia, an O^{2-} conductor) or CZI ($CaZr_{0.9}In_{0.1}O_{3-a}$, a H^{+} conductor), to the catalytic metal/gas interface. The EPOC phenomenon has been applied on a wide variety of catalysts and in a large number of important industrial and environmental catalytic reactions [17]. In particular, electrochemical promotion has been shown to enhance the catalyst activity and selectivity in the hydrogenation of CO_2 [2, 3, 6, 11, 12, 18–24]. Hence, the promotional effect may allow to in situ control the catalytic behavior of the system for syn-gas or CH_4 production via CO_2 hydrogenation. Most EPOC studies on CO_2 hydrogenation (as shown on Table 1) have been performed with a YSZ solid electrolyte and a noble metal catalyst, such as Pt, Pd, Ru and Rh [2, 3, 6, 11, 18, 20, 21, 24]. However, only a few studies have been carried out by using cationic solid electrolytes [3, 12, 19, 21–23] or non-noble metal catalysts (Ni or Cu) [2, 11, 12, 20, 22]. For practical use, is clear that the development of low-cost and highly efficient catalyst is desired. In this sense, we focused on developing an efficient catalyst film of suitable performance for the CO_2 hydrogenation reaction via electrochemical promotion by K^{+} ions. Hence, K-$b''Al_2O_3$ was selected as the solid electrolyte, and different catalyst film configurations were proposed based on Ni catalyst: (i) Ni catalyst film prepared by deposition of an organometallic paste, (ii) Ni catalyst film prepared by deposition of an slurry made by mixing a Ni metal paste and a-Al_2O_3 powder and (iii) and Ni particles dispersed on Al_2O_3 powder and deposited on the solid electrolyte using a slurry with Au paste. In this latter case the possibility of exploring the electro-promotional effect on dispersed metal nanoparticles was also examined. Hence, three different systems (Ni/K-$b''Al_2O_3$/Au, Ni–a-Al_2O_3/K-$b''Al_2O_3$/Au and Au–Ni(30 %)–a-Al_2O_3/K-$b''Al_2O_3$/Au) were studied on the basis of different characterization techniques and catalytic activity measurements under electrochemical promotion conditions. Additionally, for the selected catalytic system a kinetic study under EPOC conditions was carried out, as well as the possibility of controlling the Ni catalytic activity and selectivity toward the different obtained products (syn-gas or methane) via EPOC was investigated.

2 Experimental

2.1 Electrochemical Cell Preparation

Each electrochemical cell was based on a 19-mm-diameter, 1-mm-thick K-$b''Al_2O_3$ (Ionotec) pellet solid electrolyte. In each electrochemical cell the Au counter and reference electrodes were firstly deposited on one side of the electrolyte by annealing a gold organometallic paste (Fuel Cell Materials ref. 231001) at 800 ºC for 2 h (heating ramp of 5 ºC/min). Then, three Ni-based catalysts were prepared by different preparation methods. In the first sample (Ni/K-$b''Al_2O_3$/Au, denoted as ''N''), a coating of a commercial Ni ink (Fuel Cell Material ref. 233001) was applied on the electrolyte, followed by calcination at 800 ºC for 2 h (heating ramp of 5 ºC/min). In the second sample (Ni–a-Al_2O_3/K-bAl_2O_3/Au, denoted as ''NA''), the catalyst film was prepared by mixing 40 mg of the Ni ink with 20 mg of a commercial a-Al_2O_3, (Alfa Aesar) powder, and some ethylene glycol to obtain a slurry with suitable viscosity. Then, the slurry was deposited on the K-$b''Al_2O_3$ pellet and was subjected to the same heat treatment as that for the previous electrode (800 ºC). In the third sample (Au–Ni(30 %)–a-Al_2O_3/K-$b''Al_2O_3$/Au, denoted as ''GNA''), 40 mg of the Au ink and ethylene glycol were mixed with 20 mg of a-Al_2O_3 powder which was previously impregnated with Ni (30 % in weight) via a conventional impregnation method. The a-Al_2O_3 powder was impregnated with a $Ni(NO_3)_2 \cdot 6H_2O$ (Panreac) precursor aqueous solution in a glass vessel under vacuum at 90 ºC to yield 30 % weight of Ni. After drying overnight at 120 ºC, the resulting powder was calcined at 450 ºC (heating ramp of 5 ºC/min) for 1 h. The slurry of 30 % Ni/aAl_2O_3 ?Au ink was deposited on the solid electrolyte and annealed at 800 ºC for 2 h. In this way, it was possible to evaluate the catalytic contribution of the Ni particles dispersed on the alumina support due to the negligible activity of the Au particles coming from the ink. Table 2 summarizes the

Table 1 EPOC studies of the CO_2 hydrogenation reaction using different catalysts and solid electrolytes

Catalyst	Solid electrolyte	Catalyst film preparation technique	T (ºC)	CO_2 (%)	H_2 (%)	F_T (N mL min^{-1})	Main reaction products	EPOC behaviour	References
Rh,Pt, Cu	YSZ	Sputtering	220–380	1	5.6	100	CO, CH_4, C_2H_4	Inverted volcano	[2]
Pd	YSZ, Na–b$^{00}Al_2O_3$	Organometallic paste	533–605	72.8	22.7	38–300	CO	Inverted volcano	[3]
Rh	YSZ	Organometallic paste	346–477	5.5	63	15–50	CO, CH_4	Electrophobic (CH_4)/electrophilic (CO)	[18]
Ni, Ru	YSZ	Impregnation	200–440	1	5.6	100	CO, CH_4	Electrophilic	[11]
Ru	YSZ	Impregnation	200–300	3	30	200	CO, CH_4	Electrophobic (CH_4)/electrophilic (CO)	[6]
Pt	K-bAl_2O_3	Dip-coating	400	19–47.5	47.5–76	1500–8700	CO, CH_4, CH_3OH, C_2H_5OH, C_2 ? C_3	Electrophobic (CH_4)/electrophilic (CO). The others vary with reaction conditions	[19]
Cu	K-bAl_2O_3	Electroless deposition	200–400	19–31	63.33–76	1500–8700	CH_3OH, C_2H_5OH, C_2H_6O,	It varies with reaction conditions	[12]
Pt, Ni, Pd	YSZ	Organometallic paste/electroless	225–450	19–47.5	47.5–76	1500	CO,CH_4, CH_3OH, C_2H_6, C_3H_6, C_2H_6O	It varies with reaction conditions	[20]
Ru	YSZ K-b$^{00}Al_2O_3$	Impregnation	200–340	0.025–2	1–15	100	CO, CH_4	Electrophobic (CH_4)/electrophilic (CO)	[21]
Cu	SZY	Pd organometallic paste/Cu powder	550–750	0.6–2.24	0.3–4.9	200–300	CO	Electrophilic	[22]
Ru	K-b$^{00}Al_2O_3$	Impregnation	280–420	3	30	100	CO, CH_4	Electrophobic (CH_4)/electrophilic (CO)	[23]
Pt	YSZ	Organometallic paste	650–800	1–10	1–10	20	CO	Electrophilic	[24]

Table 2 Summary of the different Ni based electrochemical catalysts

Nomenclature	Description	Metal paste	Powder addition to the slurry	Total Ni weight (mg)	d_{metal} after reaction (nm)	N_G/active mol of Ni
N	Ni–K-b$^{00}Al_2O_3$/Au	Ni	–	17.80	39.9	9.28 9 10^{-6}
NA	Ni–aAl_2O_3/K-b$^{00}Al_2O_3$/Au	Ni	aAl_2O_3	6.17	37.5	3.43 9 10^{-6}
GNA	Au–Ni(30 %)–aAl_2O_3/K-b$^{00}Al_2O_3$/Au	Au	30.73 % Ni–aAl_2O_3	4.13	35.2	2.45 9 10^{-6}

description and nomenclature of each electrochemical catalyst along with the total Ni weight, particle size and active surface area of all catalyst electrodes. The active surface area of the catalysts, N_G, was calculated in each case by means of the total amount of deposited mol of metal and the particle diameter and dispersion values, which were estimated from the (111) XRD peak via the Scherrer equation. It can be observed that the lower the amount of Ni used, the lower the particle size. Additionally, blank experiments were carried out on a pure gold electrode (Au–K-b$^{00}Al_2O_3$/Au) and a gold paste electrode mixed with a non-impregnated alumina powder (Au–a-Al_2O_3/K-b$^{00}Al_2O_3$/Au) to confirm its negligible activity for the CO_2 hydrogenation reaction.

2.2 Electrochemical Catalyst Characterization

The different electrochemical catalysts were firstly reduced in situ during a temperature programmed reduction (TPR) experiment under a 3 % H_2 stream (N_2 balanced) of an overall flow rate of 100 N mL min^{-1}, increasing the temperature at a rate of 2 ºC/min from room temperature to 350 ºC. During the TPR, the H_2 consumption was continuously monitored by a thermal conductivity detector, whereas the in-plane Ni film surface electrical resistance between two points separated by 1 cm was measured by a digital multimeter.

After reduction, the three Ni-based catalysts were characterized by X-ray diffraction (XRD) analysis with a Philips PW-1710 instrument using Ni-filtered Cu K_a radiation (k = 1.5404 Å). Diffractograms were compared with the JCPDS-ICDD references. All catalysts were also characterized after the catalytic activity experiments to evaluate their stability under the studied reaction conditions. The morphology of the different catalyst films was also evaluated using a Quanta 250 scanning electron microscope (SEM). This instrument is equipped with an EDAX Apollo X detector (AMETEK), for determining the chemical compositions of the samples via energy-dispersive X-Ray analysis (EDAX). The Ni metal loading in the impregnated a-Al_2O_3 was determined by atomic absorption spectrophotometry, using a SPECTRA 220FS analyser. As shown in Table 2, the total amount of Ni in the powder catalyst was 30.73 % in weight.

2.3 Catalytic Activity Measurements and EPOC Parameters

The experimental setup has been described in detail in a previous work [25]. The reaction gases (Praxair, Inc.) were certified standards (99.999 % purity) of CO_2, H_2 and N_2, the latter being used as the carrier gas, and the gas flow rates were controlled by a set of mass flowmeters (Brooks 5850 E and 5850 S). The catalytic experiments were carried out at atmospheric pressure with an overall gas flow rate, F_T, ranging from 20 to 200 N mL min^{-1}, at three temperatures (T = 240, 270, and 300 ºC) and a feed composition ranging from 3 to 30 % for H_2 and from 1.5 to 10 % for CO_2 (N_2 balance). Reactant and product gases were on-line analyzed by using a micro gas-chromatograph (Varian CP-4900) equipped with two columns (Molsieve and Poraplot Q column) and two thermal conductivity detectors (TCD). The Molsieve column used Ar as carrier gas and operated at T = 80 ºC and 20 psi. On the other hand, Poraplot Q column operated at T = 70 ºC and 20 psi and used He as carrier gas. The detected reaction products were: CO, CH_4 and H_2O. The error in the carbon atom balance did not exceed 5 %. In order to carry out the electrochemical promotion (EPOC) experiments, the three electrodes (working, counter and reference) were connected to a potentiostat–galvanostat Voltalab PGZ 301 (Radiometer Analytical) using gold wires. The inertness of both the gold counter/reference electrodes and of the a-Al_2O_3 powder and Au–a-Al_2O_3 film was checked via blank experiments performed under the studied reaction conditions.

The CO_2 conversion and the CO and CH_4 selectivities were calculated as follows:

$$CO_2\ conversion(\%) = \frac{F^0_{CO_2} - F_{CO_2}}{F^0_{CO_2}} \times 100 \quad (4)$$

$$CO\ selectivity(\%) = \frac{F_{CO}}{F^0_{CO_2} - F_{CO_2}} \times 100 \quad (5)$$

$$CH_4\ selectivity(\%) = \frac{F_{CH_4}}{F^0_{CO_2} - F_{CO_2}} \times 100 \quad (6)$$

where F^0_i and F_i are the molar flow rates of the i species at the inlet and at the outlet of the reactor, respectively. On the other hand, the magnitude of the electropromotional

effect was quantified by two parameters commonly used in this kind of studies:

– The rate enhancement ratio of each compound (q_i), defined by the equation:

$$q_i = \frac{r_i}{r_{i;0}} \quad (7)$$

where r_i and $r_{i,0}$ are the promoted (U_{WR} \ 2 V) and reference (unpromoted) state (U_{WR} = 2 V) catalytic production rates, respectively, of the corresponding compound.

– The promotion index ($PI_{K?}$), calculated by the equation:

$$PI_{K?} = \frac{\frac{Dr}{r_0}}{\theta_{K?}} \quad (8)$$

where Dr = r - r_0 is the potassium-induced change in catalytic reaction rate and $h_{K?}$ is the potassium coverage calculated from the integration of the current (I) versus time (t) curves according to the Faraday law (Eq. 9):

$$\theta_{K?} = \frac{\int_0^t I dt}{nFN_G} \quad (9)$$

where n is the potassium ion charge, i.e., ?1, F is the Faraday constant (96484.6 C/mol), and N_G is the active mol of the Ni catalysts, which was calculated in each case by means of the total amount of deposited Ni and the particle diameter and dispersion values estimated from the (111) from XRD analysis peak via Scherrer equation.

3 Results and Discussion

3.1 Influence of the Preparation Method of the Catalyst Film

Figure 1 shows the variation of the surface electrical resistance of the Ni catalyst film and the H_2 consumption rate during the temperature programmed reaction experiment (TPR) for sample N. During the TPR experiments, no significant differences were appreciated between the two electrochemical catalysts based on the Ni catalyst film (N, and NA). For sample N, it can be observed that at the beginning of the experiment, the as-deposited Ni catalyst film showed a very high value of the electrical resistance (125 LX). This seems to indicate that the catalyst preparation method (involving calcination at high temperature under air atmosphere) led to an oxidized nickel film (as will be shown below by XRD data). However, following the

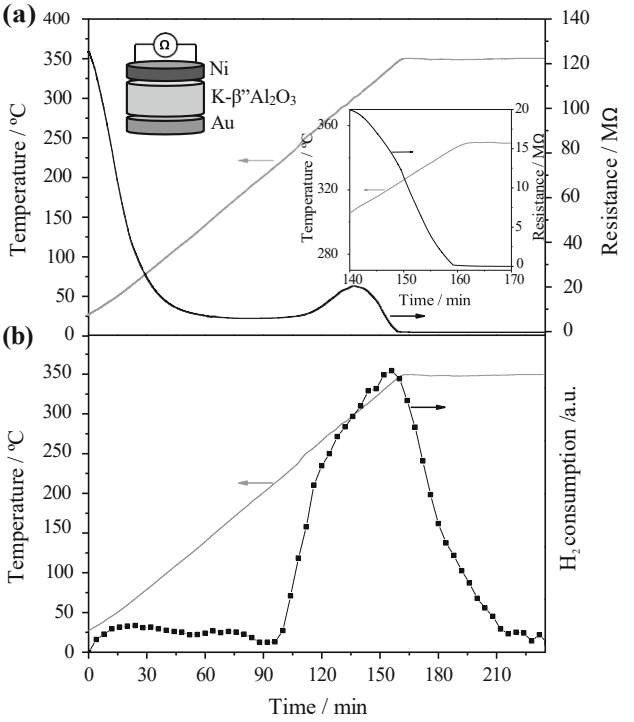

Fig. 1 Variation of Ni surface electrical resistance (a) and H_2 consumption rate (b) during the TPR experiment for catalyst N. Inset of (a) shows the final variation of Ni electrical resistance and temperature with time. Heating rate of 2 ºC/min under a 3 % H_2 stream (N_2 balance)

TPR experiment the electrical resistance decreased and finally stabilized at only 0.3 X after 1 h at 350 ºC which indicated complete reduction of the catalyst film to metallic Nickel (as will be shown below by XRD data), in agreement with previous works using Ni catalysts [26–28]. This reduction process can be confirmed by the H_2 consumption peak which started at around 250 ºC. The initial decrease in the electrical resistance of the Ni catalyst film with temperature (25–125 ºC) with no parallel H_2 consumption could be attributed to the semiconducting properties of NiO [29]. On the other hand the appearance of a local maximum value in the film resistance around 300 ºC could be explained by the partial formation of different intermediate Ni oxides of lower electrical conductivity. However, the catalyst surface composition in the course of the TPR experiment is unknown.

Figure 2 shows the crystalline structure of the different Ni-based catalysts, namely N (Fig. 2a), NA (Fig. 2b) and GNA (Fig. 2c), analysed by XRD both after the in situ TPR up to 350 ºC (*fresh catalyst*, top spectra) and after exposure to all the studied reaction conditions (*used catalyst*, bottom spectrum). For the case of sample N, the XRD analysis before reduction (TPR) is also included on Fig. 2a. In this latter case it can be observed that the Ni catalyst film was mainly in its oxidized state (NiO and NiO_2, JCPDS,

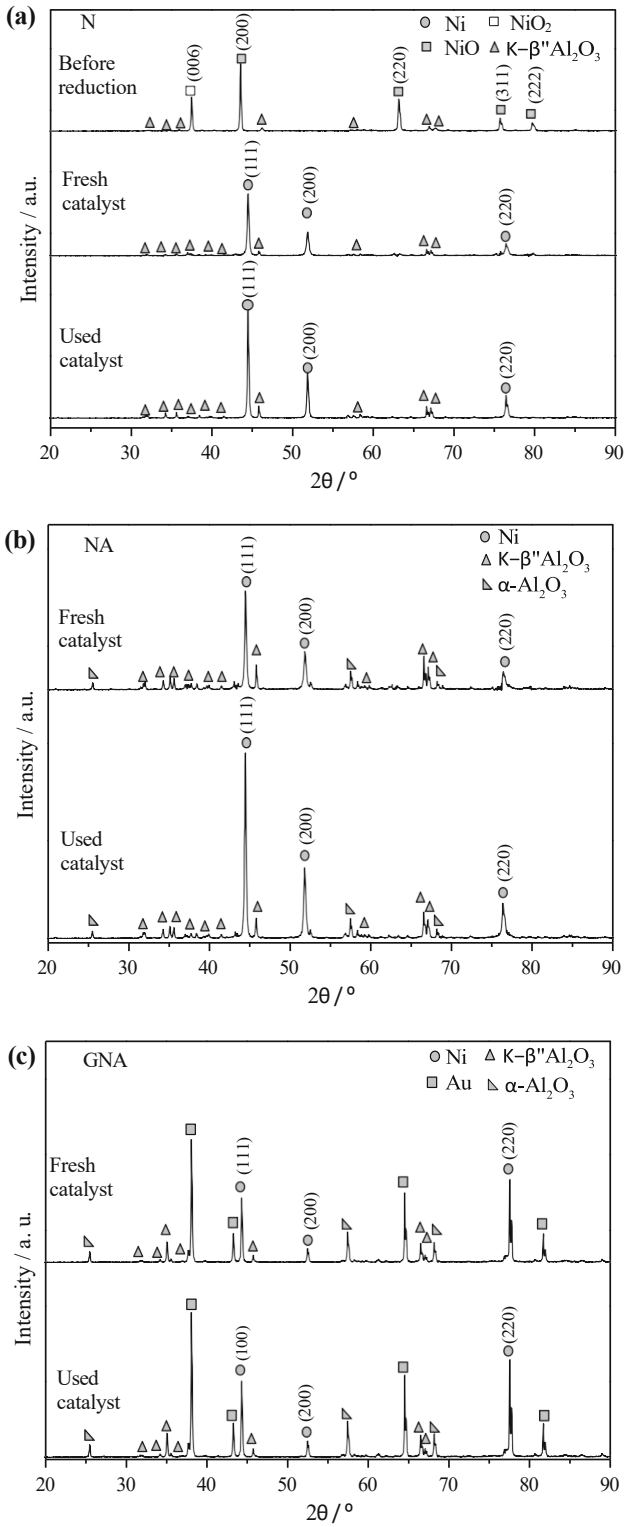

Fig. 2 XRD analysis patterns of catalysts a N, b NA and c GNA before and after exposure to reaction conditions. For catalyst N (a), the XRD analysis pattern before reduction is also included

78-0643 and JCPDS, 85-1977, respectively), which is in in agreement with the electrical resistance measurements during TPR, shown in Fig. 1. However, the Ni catalyst films were completely reduced during the TPR experiments since no patterns of nickel oxides appeared in any of the fresh catalysts (after reduction and before activity measurements). In all cases the main diffraction peaks (111), (200) and (220) which appeared at 2h = 44.5º, 51.8º and 76.4º, respectively, were associated with metallic nickel and corresponded to a face-centered cubic (FCC) crystalline structure (JCPDS, 87-0712). Diffraction peaks related to the K-b$^{00}Al_2O_3$ solid electrolyte (JCPDS, 02-0921) were found in all spectra, whereas samples NA and GNA (Fig. 2b, c, respectively) also exhibited the peaks corresponding to a-Al_2O_3 (JCPDS, 01-1296). In addition, reflections appearing at 38º, 44º, 64º and 82º in Fig. 2c corresponded, respectively, to the (111), (200), (220) and (222) planes of metallic gold (JCPDS, 01-1172) in sample GNA. Remarkably, the reduced state of the Ni catalysts remained during the catalytic experiments due to the presence of H_2 in the feed. Additionally, the intensity of the Ni XRD peaks (111, 200, and 220) for the used samples of catalyst N and NA (Fig. 2a, b, respectively) slightly increased compared to those for the fresh samples, as observed in post-reaction XRD spectra (denoted in all the cases as used catalyst). However, the particle size of Ni (estimated using the Scherrer equation) before and after the experiments was practically the same in all cases. This indicated the stability of the catalyst under experimental conditions, also supported by the good reproducibility observed in its catalytic performance in the reference (unpromoted) state (application of ?2 V), as will be shown below.

A Ni particle size of 39.9 nm was estimated for the N catalyst (Table 2), which decreased in the NA and GNA samples. These values were of the same order with those reported in other EPOC studies with Ni catalysts prepared by different techniques [11, 20] and should imply a high catalytic activity [1, 19]. Aside from the approximate character of this calculation, the addition of the alumina powder to the Ni and Au pastes slightly decreased de metal particle size and very likely increased the Ni particles dispersion. On the other hand, a very slight increase in the particle size was observed after the experiments in all cases (particle size before reaction equal to 38.9, 36.5 and 34.7 nm for catalyst N, NA and GNA, respectively), which denoted a minimal thermal sintering effect on all catalysts under the studied reaction conditions. SEM micrographs and EDAX analysis of certain regions of the different Ni catalyst-electrodes obtained after exposure to reaction conditions are shown in Fig. 3. It can be observed that all samples were porous, which facilitated the reactants and products diffusion. However, it can also be observed that the catalyst preparation method (by the addition of a powder to the ink) markedly influenced its surface composition and morphology. From Fig. 3a1, a2 (sample N),

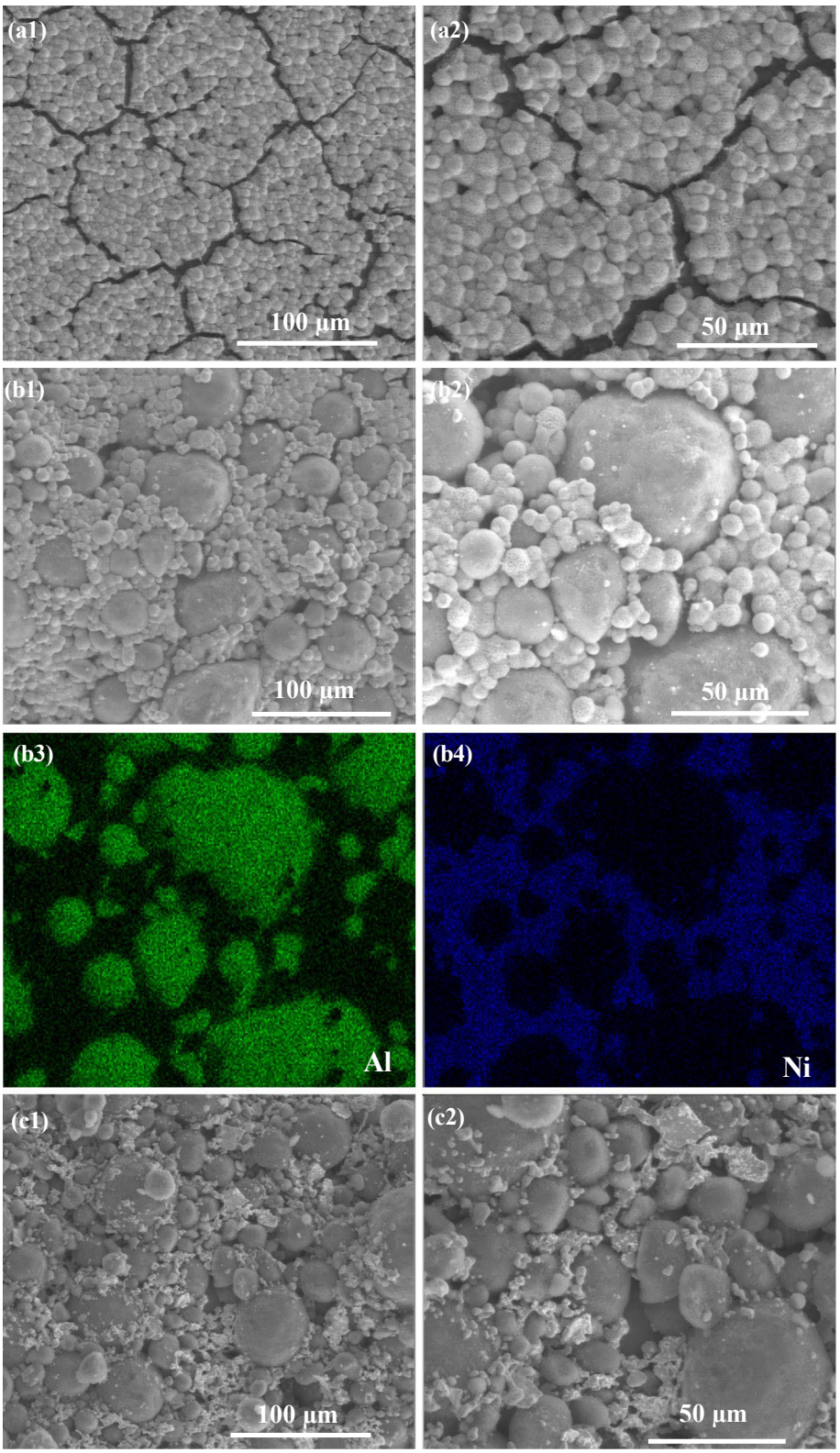

Fig. 3 SEM micrographs of catalysts a N, b NA and c GNA after exposure to reaction conditions. EDAX mapping is also included for catalysts NA

the obtained Ni film seems to resemble a typical homogeneous foam structure with big Ni agglomerates ranging from 6.0 to 7.0 lm [26, 30]. However, two components can be clearly distinguished in sample NA (Fig. 3b1, b2); Ni agglomerates with similar morphology than those present in sample N (Fig. 3a2) and larger size particles with a

smooth surface which corresponded with the a-Al_2O_3 powder. These particles of a-Al_2O_3 were round shaped, with a typical size distribution ranging between 30 and 65 lm. Moreover, an elemental mapping of Fig. 3b2 was performed as shown on Fig. 3b3, b4 corresponding to Al and Ni, respectively. It is clear that the previously mentioned largest particles were composed of Al (in green, Fig. 3b3) and O (not shown), thus corresponding to the a-Al_2O_3 powder, while the smallest agglomerates mainly contained Ni (in blue, Fig. 3b4). It can also be observed that sample NA exhibited a larger roughness (porosity) and a higher number of valleys and holes in comparison with sample N, due to the presence of the heterogeneous particles of a-Al_2O_3. Hence, it is very likely that the incorporation of a-Al_2O_3 powder allows re-dispersion of the Ni particles coming from the ink, leading to an increase of the catalytic surface area, as already shown in a previous study with Pt ink [31], and demonstrated by an increase in the metal dispersion (3, 3.4 and 3.5 % for catalyst N, NA and GNA, respectively. Finally, sample GNA (Fig. 3c1, c2) showed a similar porous structure with sample NA formed by the Au particles coming from the Au ink and the a-Al_2O_3 powder.

In order to select the most suitable Ni catalyst preparation method for CO_2 hydrogenation via EPOC, all samples (N, NA and GNA) were tested under certain reaction conditions and potentials (U_{WR}) ranging from ?2 to -2 V. Figure 4 shows the dynamic response of the reaction rates for CO_2 consumption, CO and CH_4 formation for each catalyst (N, NA and GNA) and of the electrical current obtained upon catalyst potential variation for catalyst N. During the measurement of transient currents, no significant differences were appreciated between the three electrochemical catalysts (N, NA and GNA). All reported rate values were normalized to the total mol of deposited Ni. These experiments were carried out at 240 ºC with a feed composition of H_2/CO_2 = 30 %/1.5 % (N_2 balance) and an overall flow rate of 100 N mL min^{-1}. The electropromotional behavior was the same for the case of sample N and NA (no electro-promotional effect was observed for sample GNA). Firstly, the application of a positive potential U_{WR} = ?2 V (reference state) at the beginning and at the end of each experiment (as well as before each negative polarization) ensured the removal of K? ions from the catalyst surface which had previously migrated to the catalyst surface by thermal migration [3, 32]. Thus, as shown in Fig. 4d, following application of a constant voltage the generated current decreases with time to values close to zero indicating that a steady state coverage of potassium is achieved after certain time. In this way, a reference state was obtained and the reversibility of the electropromoted effect was checked. At the reference state (U_{WR} = ?2 V), CO and CH_4 were already produced by means of the

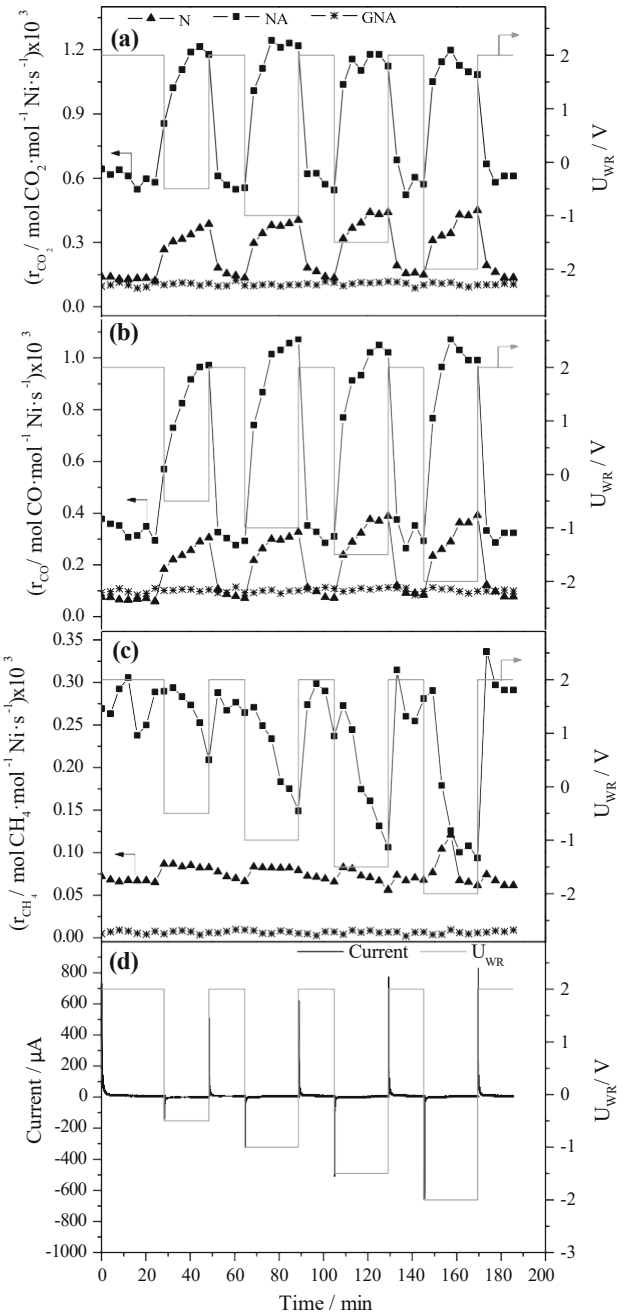

Fig. 4 Influence of the applied potential vs. time on the reaction rate values of a CO_2 consumption, b CO production and c CH_4 production with the different catalysts (N, NA and GNA) and obtained electric current d versus time to step changes in the applied catalyst potential U_{WR} for catalyst N. Reaction conditions: H_2/CO_2 = 30 %/1.5 % (N_2 balance), F_T = 100 N mL min^{-1}, T = 240 ºC

reverse water–gas shift (Eq. 2) and CO_2 methanation (Eq. 3) reactions, respectively. Then, the subsequent decrease in the applied catalyst potential increased the amount of K? ions that migrated electrochemically from the K-b^{00}Al_2O_3 pellet to the catalyst surface (promoted state), according to the obtained negative current (Fig. 4d). As a consequence, the overall reaction rate of CO_2

increased as well as the production rate of CO, while the production rate of CH_4 decreased for the case of samples N and NA. According to previous EPOC studies on CO_2 hydrogenation [6, 18, 19, 21], the RWGS reaction is electrophilic, i.e., the CO production rate increases with decreasing potential (i.e., with increasing $K^?$ coverage). In parallel, an electrophobic behaviour for the methanation reaction was typically observed, i.e., the CH_4 production rate increased with increasing potential and decreasing amount of supplied $K^?$ promoter. The obtained results with the N and NA samples were consistent with the general rules of chemical and electrochemical promotion [17]. In the present work, for these two samples the migration of $K^?$ onto the catalyst-working electrode would weaken the chemical bond of Ni with the electron donor adsorbates (hydrogen) and strengthen that with the electron acceptors (CO_2). The increase in the binding strength of CO_2 on the Ni surface would favour the dissociative adsorption of CO_2 through the RWGS reaction rather than CO_2 methanation. Hence, the presence of $K^?$ ions on the catalyst-film led to a strong promotional effect in the CO_2 hydrogenation mechanism toward CO formation. This effect has also been reported in several previous studies of chemical and electrochemical promotion with $K^?$ ions on different metal catalysts [12, 19, 21, 33, 34]. Moreover, it should be noted that for both samples N and NA, the electropromotional effect after each polarization at ?2 V showed to be fully reversible and reproducible in terms of catalytic activity. This demonstrates the great advantage of the EPOC effect compared to the conventional chemical promotion, by providing full control and optimization of the promoted state of the catalyst in the course of the reaction [13].

On the other hand, it is interesting to note that sample NA showed the higher catalytic activity in terms of reaction rate normalized per amount of deposited Ni for all the applied catalyst potentials between ?2 and −2 V. This catalytic enhancement derived from the powder addition can be explained considering the increase in the Ni ink porosity, as mentioned above. Catalyst NA was overall found to be the most active catalyst. Regarding the results obtained with catalyst GNA, it must be taken into account that both the pure gold electrode and the gold paste mixed with non-impregnated alumina powder showed complete inactivity under all the studied reaction conditions (as well as negligible electro-promotional effect). Hence, the residual activity of catalyst GNA can be attributed to the presence of Ni particles impregnated on the powder since negligible activity was observed on a Au film prepared with inert a-Al_2O_3 for blank experiments (not shown). Hence, the obtained results shown in Fig. 4 confirm the absence of any electro-promotional effect related to the Ni particles dispersed on a-Al_2O_3. This can be explained considering the absence of conduction pathways of $K^?$ ions from the solid electrolyte to reach the Ni particles dispersed on the a-Al_2O_3 support. Summarizing, Ni metal particles provided by the deposited metal ink (and not the impregnated Ni particles) were the active catalyst and were also electrochemically promoted for the CO_2 hydrogenation reaction. According to the aforementioned results, all the electrochemical promotion experiments described in the next section were performed with catalyst NA.

3.2 Kinetic Study and Electrochemical Promotion Experiments

Figure 5 shows the effect of gas flow rate, F_T, on the CO_2 reaction rate, CO_2 conversion and selectivity to CO and CH_4 at the reference state, U_{WR} = 2 V, and different feed compositions. The reference (unpromoted) catalytic rate initially increased with increasing flow rate and reached a plateau at high flow rate values (F_T [75 N mL min^{-1}). This indicates the absence of any mass transfer limitation phenomena above this flow rate. Hence, all the catalytic experiments hereafter were carried out at 100 N mL min^{-1}. As expected, the CO_2 conversion values decreased continuously upon increasing the flow rate and, very interestingly, the CH_4 selectivity also followed a negative trend. This seems to suggest that CH_4 was rather produced, to a large extent, from CO hydrogenation (Eq. 10), as a consecutive step of the RWGS reaction, than from the direct CO_2 methanation reaction (Eq. 3).

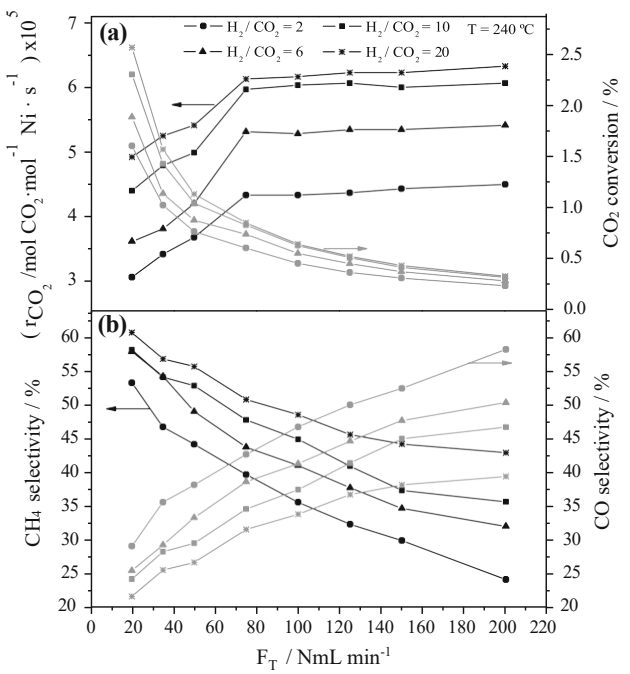

Fig. 5 Effect of the overall gas flow rate on the a CO_2 consumption rate and CO_2 conversion, b CH_4 and CO selectivity under ?2 V polarization for catalyst NA. Reaction conditions: H_2/CO_2 = 30 %/ 1.5 % (N_2 balance), T = 240 ºC

$CO + 3H_2 \rightarrow CH_4 + H_2O$ (10)

In fact, concerning the kinetics of the reactions, reaction rate of CO_2 methanation is generally considered to be slower than reaction rate of CO methanation [35]. Furthermore, it can also be observed that an increase in the hydrogen concentration led to higher CO_2 conversion and CH_4 selectivity, which will be discussed below in more detail.

Figures 6 and 7 show the steady state effect of applied potential on the reaction rates of CO_2, CO and CH_4 at 240 ºC under different H_2 feed composition, H_2 = 3–30 %, (Fig. 6) and CO_2 feed composition, CO_2 = 1.5–10 % (Fig. 7). In all cases a cathodic (negative) polarization increased the reaction rate of CO production (electrophilic behaviour) while an anodic (positive) polarization enhanced the reaction rate of CH_4 formation (electrophobic behaviour). Since, for all the experiments, the potential-induced change of CO production rate was more pronounced than that of CH_4, the overall reaction rate of CO_2 was found to increase with negative polarization (overall electrophilic behaviour). Besides, very useful information on the reaction kinetics at the reference state can be extracted from these two figures, which can be then correlated with the electrochemical promotion behaviour observed in these experiments. In the absence of K? promoter (positive polarizations), the rate of CO formation exhibited a zero to negative order with respect to H_2 concentration (Fig. 6) and a marked positive order with respect to CO_2 concentration (Fig. 7). On the contrary, the rate of CH_4 formation showed a positive order with respect to H_2 and a negative to zero order with respect to CO_2. As a direct consequence, the CO_2 reaction rate was positive order with respect to both H_2 and CO_2. Similar trends were observed in other EPOC studies of CO_2 hydrogenation [6, 18]. Hence, in view of these results, one could easily explain the EPOC behaviour observed upon varying the catalyst potential. As mentioned above, CO production through RWGS was favoured by increasing CO_2 feed concentration, which is equivalent to increasing the CO_2 chemisorption strength on the Ni surface via alkali electrochemical promotion. On the other hand, since methanation reaction at the reference state was already inhibited by increasing the CO_2 feed concentration, it is expected that the potassium backspillover at negative potentials and the consequent strengthening of the CO_2 chemisorption also resulted in decrease of the methane formation rate. Hence, RWGS is an electrophilic reaction, i.e., it is positive order in the electron acceptor reactant (CO_2) and negative or zero order in the electron donor reactant (H_2), while CO_2 methanation is an electrophobic reaction, i.e., it is zero to negative order in CO_2 and positive order in H_2 [18, 21]. Thus, it is clear that the EPOC phenomena allow to control

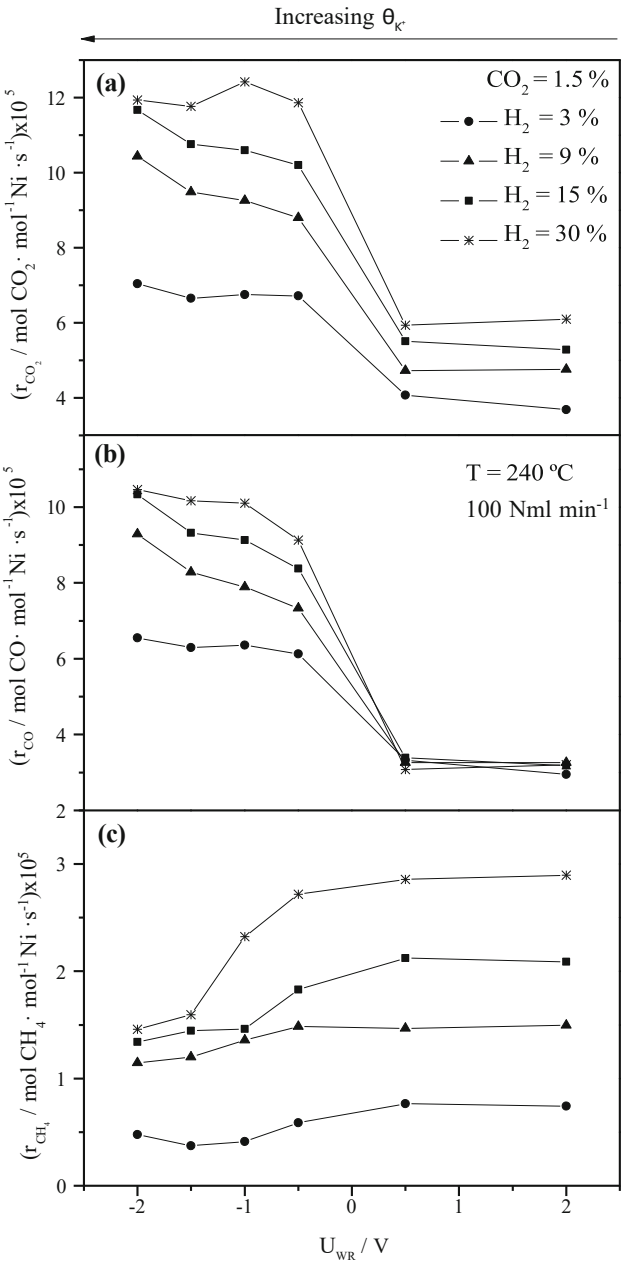

Fig. 6 Effect of the H_2 concentration on the reaction rate values of a CO_2 consumption, b CO production and c CH_4 production under different applied potentials (U_{WR}) for catalyst NA. Reaction conditions: CO_2 = 1.5 % (N_2 balance), F_T = 100 N mL min^{-1}, T = 240 ºC

in situ the competitive chemisorption of the different adsorbates on the catalyst surface which may allow control of the selectivity requirements as will be shown below.

Figure 8 depicts the effect of temperature on reaction rates of CO_2, CO and CH_4 for a feed composition of H_2/CO_2 = 30 %/1.5 % (N_2 balance). At the reference (unpromoted catalyst) state (U_{WR} = 2 V) and under electropromoted (U_{WR} \ 2 V) conditions, it can be observed that

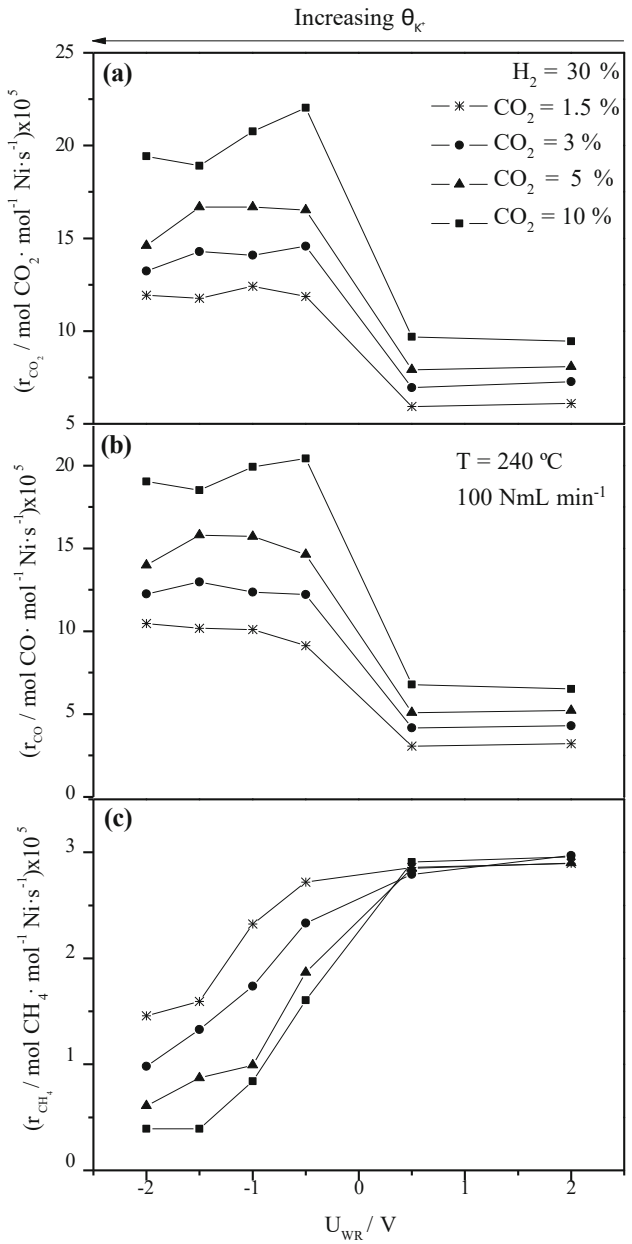

Fig. 7 Effect of the CO_2 concentration on the reaction rate values of a CO_2 consumption, b CO production and c CH_4 production under different applied potentials (U_{WR}) for catalyst NA. Reaction conditions: H_2 = 30 % (N_2 balance), F_T = 100 N mL min^{-1}, T = 240 ºC

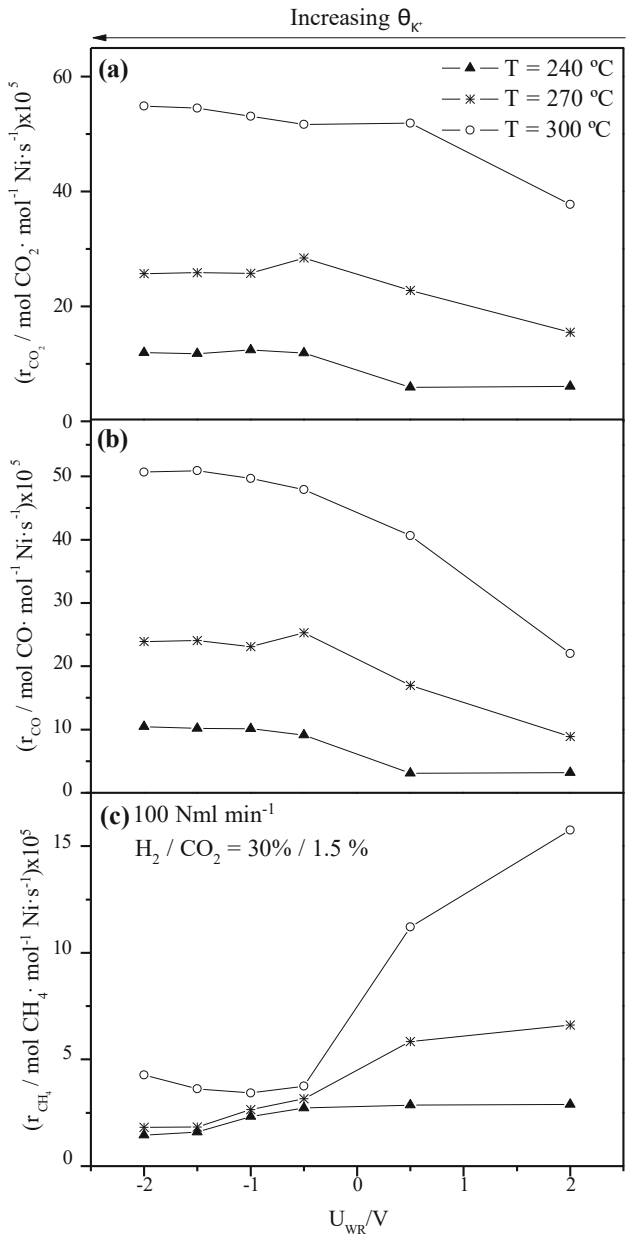

Fig. 8 Effect of temperature on the reaction rate values of a CO_2 consumption, b CO production and c CH_4 production under different applied potentials (U_{WR}) for catalyst NA. Reaction conditions: H_2/CO_2 = 30 %/1.5 % (N_2 balance), F_T = 100 N mL min^{-1}

the reaction rate of CO_2, as well as the production rate of CO and CH_4 were enhanced by increasing temperature. A similar positive effect of temperature was also observed in other EPOC studies with different metal catalysts [11, 18, 22, 24]. At all temperatures, the same EPOC behavior of the RWGS and methanation reactions was found (previously discussed at 240 ºC), i.e., electrophilic CO and electrophobic CH_4 production, respectively. Moreover, it is important to note that the Ni catalyst was activated via electrochemical promotion in such a way that a very similar production rate of CO was achieved under promoted conditions at 240 and 270 ºC as observed in the absence of promoter at 270 and 300 ºC, respectively. Hence, the application of an electric potential which corresponds to a current of the order of a few lA may cause a similar modification in the catalytic performance as a temperature increase of 30 ºC. This demonstrates the great practical interest of the EPOC phenomenon in view of energy savings, by activating a metal catalyst at lower temperatures

[13, 36, 37]. Finally, the apparent activation energy calculated via the Arrhenius plot at the reference state (U_{WR} = 2 V) was 74.26 kJ mol^{-1} for CO_2 consumption. This value is in the same range as those reported in other works. For instance, an activation energy of 40–80 kJ mol^{-1} was reported for the hydrogenation of CO_2 over Ni catalyst [11]. Peebles et al. obtained activation energies of 88.7 and 72.8–82.4 kJ mol^{-2} for the methanation and dissociation of CO_2 on Ni (100) for producing CH_4 and CO, respectively [38]. On the other hand, an activation energy of 62.14 kJ mol^{-1} was obtained for CO_2 consumption under electro-promoted conditions (-2 V). The activation energy was reduced from 74.26 kJ mol^{-1} (reference state) to 62.14 kJ mol^{-1} (promotion conditions) which demonstrates the positive effect of K? ions on the kinetics of the process, as already concluded in other previous works of potassium-electropromotion [39, 40].

Figure 9 shows the variation of the reaction rate enhancement ratio (q_i), calculated for CO_2, CO and CH_4 through Eq. 7, with the applied potential, under a feed composition of H_2/CO_2 = 30 %/1.5 % (N_2 balance) and three different reaction temperatures. The corresponding promotional indexes ($PI_{K?}$, Eq. 8) are also shown for an applied potential of -0.5 V. At all studied temperatures, a clear electrophilic EPOC effect can be observed in the global CO_2 reaction and the CO production (q [1, $PI_{K?}$ [0), due to the previously explained promotional effect K? ions at negative potentials. The electrophobic behavior of CH_4 formation rate was also verified (q \ 1, $PI_{K?}$ \ 0). Hence, CO showed the highest promotion index values, as well as the most pronounced increase in the reaction rate with respect to the reference state. The higher the reaction temperature, the lower the values of the rate enhancement ratio, which was associated to the concomitant increase in the reference reaction rates (r_0). For the case of the promotional index, the maximum values were obtained at 270 ºC, since it depended on the relative increase of the catalytic rates and potassium coverages. This could be attributed to the increase in the ionic conductivity of the solid electrolyte, and hence in potassium coverage at fixed potential, with increasing temperature.

Finally, in Fig. 10 is shown the influence of the applied potential on the steady-state variation of the selectivity towards CO and CH_4 at different temperatures (T = 240, 270 and 300 ºC) and different feed composition (H_2/CO_2 = 2–20). At all temperatures the decrease in the applied potential resulted in a strong increase of CO selectivity (Fig. 10a2–c2) and a decrease of CH_4 selectivity (Fig. 10a1–c1). For instance, with a H_2/CO_2 ratio of 20, the selectivity of the Nickel catalyst towards CO production was enhanced up to more than 95 % with a potassium coverage, $h_{K?}$, between 0.019 and 0.066, depending on the reaction temperature. As reported in previous EPOC studies on CO_2 hydrogenation

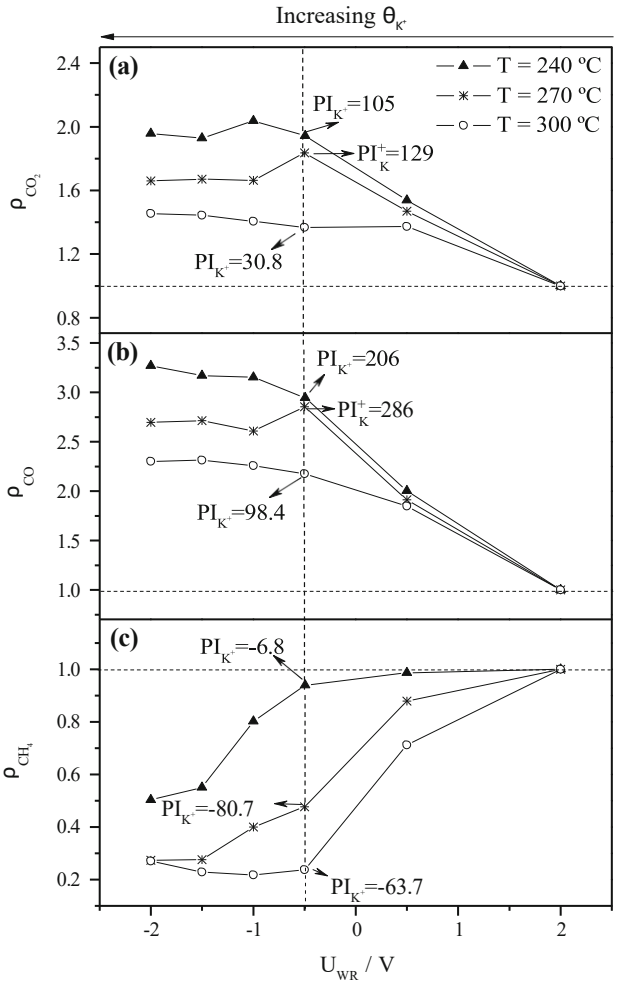

Fig. 9 Effect of the applied potential (U_{WR}) on the rate enhancement ratio (q_i) of a CO_2, b CO and c CH_4 at different temperatures (T = 240, 270 and 300 ºC), with H_2/CO_2 = 30 %/1.5 % (N_2 balance) and F_T = 100 N mL min^{-1} for catalyst NA. The promotional index ($PI_{K?}$) values are also depicted for an applied potential of -0.5 V. Data obtained from the experimental results shown in Fig. 7

[12, 19, 21, 23], the activity and selectivity of other metallic catalysts were also in situ modified by pumping alkali ions. A value of 75 % in methane selectivity at T = 300 ºC (H_2/CO_2 = 7) was reported by Theleritis et al., [21]. In the present work, at the reference (unpromoted) state, a selectivity value of 50 % was obtained. Although the methane selectivity value obtained in this study was lower, the main advantage to be highlighted here is the use of a non-noble metal catalyst (Ni). Moreover, the CH_4 production rate was increased over CO production rate at higher H_2 concentrations, in good agreement with the previous discussion and other CO_2 hydrogenation studies [6, 19, 22, 41]. The decrease in temperature also enhanced the methanation selectivity, as reported in other works of conventional chemical promotion [42] and electrochemical promotion [6, 11, 21]. Depending on both the applied potential and the

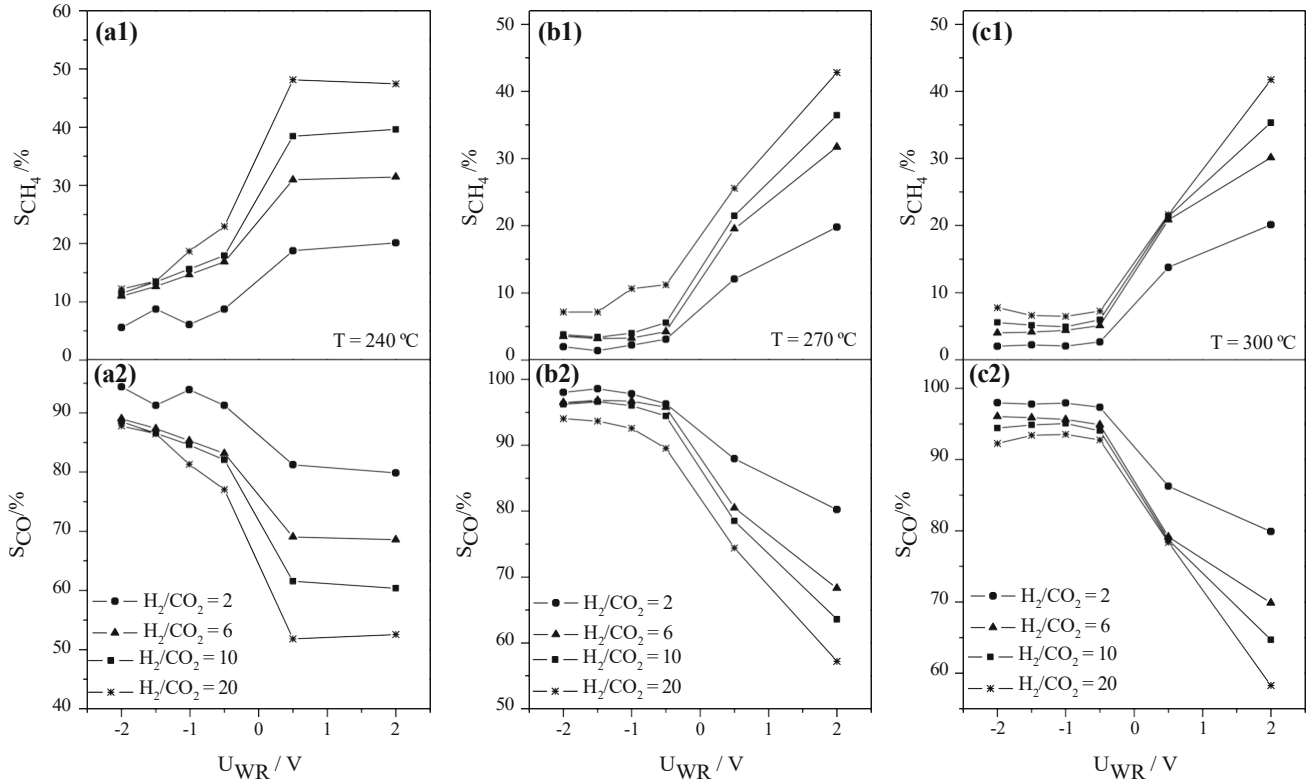

Fig. 10 Effect of the applied potential (U_{WR}) and H_2/CO_2 ratio feed concentration on the selectivity of CH_4 and CO, at a 240 ºC, b 270 ºC and c 300 ºC for catalyst NA. Reactions conditions: F_T = 100 N mL min^{-1}

reactions conditions, one can control the Ni catalytic activity and the selectivity towards CO and CH_4 by means of the controlled migration of K? ions from a solid electrolyte.

4 Conclusions

- Different Ni catalysts films were prepared on K-b00Al_2O_3 by combining organometallic paste deposition and addition of a-Al_2O_3 powder, and tested in the CO_2 hydrogenation reaction. The addition of a-Al_2O_3 powder to the Ni ink resulted in a slight increase of the catalyst film porosity, as revealed in SEM images, which resulted in a higher catalytic activity.
- The Ni catalyst films were stable under the studied reaction conditions. The Ni catalyst remained in its reduced state during the catalytic tests and the Ni particle size was stable, as confirmed by XRD analysis. This suggested that the possible thermal sintering effect was negligible, leading to a reversible EPOC behaviour between the different potentiostatic transitions.
- Both the activity and selectivity of the catalysts were in situ modified by the controlled electrochemical migration of K? ions from the solid electrolyte (electro-active catalyst support). The reverse water–gas shift and methanation reactions exhibited electrophilic and electrophobic EPOC behaviours, respectively, since negative polarizations promoted the production of CO and decreased the CH_4 production rate.
- In good agreement with the obtained catalytic results and with the rules of chemical and electrochemical promotion, the kinetic experiments confirmed that CO production was positive order with respect to the electron acceptor reactant (CO_2) and negative to zero order with respect to the electron donor reactant (H_2).
- The catalytic selectivity of Ni can be strongly modified and controlled by the application of an electric potential. Depending on the reaction conditions, CO and CH_4 selectivity was enhanced up to more than 95 and 45 %, respectively, via EPOC. Hence, one could in situ control the preferential formation of syngas or CH_4 production rate via CO_2 hydrogenation, which may be of significant practical importance.

Acknowledgments Financial Support from the Spanish ‘‘Ministerio de Ciencia e Innovacio´n’’ (CTQ2013-45030-R) and from Abengoa Research is gratefully acknowledged.

References

1. Wang W, Wang S, Ma X, Gong J (2011) Chem Soc Rev 40:3703–3727
2. Papaioannou EI, Souentie S, Hammad A, Vayenas CG (2009) Catal Today 146:336–344
3. Bebelis S, Karasali H, Vayenas CG (2008) Solid State Ionics 179:1391–1395
4. Ma J, Sun N, Zhang X, Zhao N, Xiao F, Wei W, Sun Y (2009) Catal Today 148:221–231
5. Baiker A (2000) Appl Organomet Chem 14:751–762
6. Theleritis D, Souentie S, Siokou A, Katsaounis A, Vayenas CG (2012) ACS Catal 2:770–780
7. Lapidus AL, Gaidai NA, Nekrasov NV, Tishkova LA, Agafonov YA, Myshenkova TN (2007) Pet Chem 47:75–82
8. Marwood M, Doepper R, Renken A (1997) Appl Catal A 151:223–246
9. Schild C, Wokaun A, Baiker A (1990) J Mol Catal 63:243
10. Vesborg PCK, Chorkendorff I, Knudsen I, Balmes O, Nerlov J, Molenbroek AM, Clausen BS, Helveg S (2009) J Catal 262:65
11. Jime´nez V, Jime´nez-Borja C, Sa´nchez P, Romero A, Papaioannou EI, Theleritis D, Souentie S, Brosda S, Valverde JL (2011) Appl Catal B 107:210–220
12. Ruiz E, Cillero D, Mart´ınez PJ, Morales A´, Vicente GS, De Diego G, Sa´nchez JM (2014) Catal Today 236:108–120
13. de Lucas-Consuegra A (2015) Catal Surv Asia 19:25–37
14. Choi P, Jun K-W, Lee S-J, Choi M-J, Lee K-W (1996) Catal Lett 40:115–118
15. Cubeiro MJ, Valderrama G, Goldwasser MR, Gonzalez-Jimenez F, da Silva MC, Perez-Zurita MJ (1998) Stud Surf Sci Catal 107:231
16. Stoukides M, Vayenas CG (1981) J Catal 70:137
17. Vernoux P, Lizarraga L, Tsampas MN, Sapountzi FM, De Lucas-Consuegra A, Valverde J-L, Souentie S, Vayenas CG, Tsiplakides D, Balomenou S, Baranova EA (2013) Chem Rev 113:8192–8260
18. Bebelis S, Karasali H, Vayenas CG (2008) J Appl Electrochem 38:1127–1133
19. Ruiz E, Cillero D, Mart´ınez PJ, Morales A´, Vicente GS, de Diego G, Sa´nchez JM (2013) Catal Today 210:55–66
20. Ruiz E, Cillero D, Mart´ınez PJ, Morales A´, Vicente GS, De Diego G, Sa´nchez JM (2014) J CO2 Util 8:1–20
21. Theleritis D, Makri M, Souentie S, Caravaca A, Katsaounis A, Vayenas CG (2014) ChemElectroChem 1:254–262
22. Karagiannakis G, Zisekas S, Stoukides M (2003) Solid State Ionics 162–163:313–318
23. Makri M, Katsaounis A, Vayenas CG (2015) Electrochim Acta. doi:10.1016/j.electacta.2015.03.144
24. Pekridis G, Kalimeri K, Kaklidis N, Vakouftsi E, Iliopoulou EF, Athanasiou C, Marnellos GE (2007) Catal Today 127:337
25. de Lucas-Consuegra A, Gutie´rrez-Guerra N, Caravaca A, Serrano-Ruiz JC, Valverde JL (2014) Appl Catal A 483:25–30
26. de Lucas-Consuegra A, Caravaca A, Gonza´lez-Cobos J, Valverde JL, Dorado F (2011) Catal Commun 15:6–9
27. Ho SC, Chou TC (1995) Ind Eng Chem Res 34:2279–2284
28. Sa J, Kayser Y, Milne CJ, Abreu Fernandes DL, Szlachetko J (2014) PCCP 16:7692–7696
29. Guziewicz M, Grochowski J, Borysiewicz M, Kaminska E, Domagala JZ, Rzodkiewicz W, Witkowski BS, Golaszewska K, Kruszka R, Ekielski M, Piotrowska A (2011) Opt Appl 41:431–440
30. Kim SH, Chung JH, Kim YT, Han J, Yoon SP, Nam SW, Lim TH, Lee HI (2010) Int J Hydrog Energy 35:3136–3140
31. de Lucas-Consuegra A, Caravaca A, Mart´ınez PJ, Endrino JL, Dorado F, Valverde JL (2010) J Catal 274:251–258
32. Dorado F, de Lucas-Consuegra A, Vernoux P, Valverde JL (2007) Appl Catal B Environ 73:42–50
33. Clarke DB, Bell AT (1995) J Catal 154:314–328
34. Millar GJ, Rochester CH, Waugh KC (1995) J Catal 155:52–58
35. Willauer HD, Ananth R, Olsen MT, Drab DM, Hardy, Williams FW (2013) J CO2 Util 3–4:56–64
36. de Lucas-Consuegra A, Princivalle A, Caravaca A, Dorado F, Guizard C, Valverde JL, Vernoux P (2010) Appl Catal B 94:281–287
37. de Lucas-Consuegra A, Dorado F, Jime´nez-Borja C, Valverde JL (2008) Appl Catal Environ 78:222–231
38. Peebles DE, Goodman DW, White JM (1983) J Phys Chem 87:4378–4387
39. Coulter K, Goodman DW, Moore RG (1995) Catal Lett 31:1–8
40. de Lucas-Consuegra A, Dorado F, Valverde JL, Karoum R, Vernoux P (2007) J Catal 251:474–484
41. Goodman DJ (2013) Methanation of carbon dioxide. Thesis, University of California, Los Angeles
42. Liu J, Li C, Wang F, He S, Chen H, Zhao Y, Wei M, Evans DG, Duan X (2013) Catal Sci Technol 3:2627–2633